Astron. Astrophys. 360, 49–56 (2000)

ASTRONOMY AND ASTROPHYSICS

Probing circumnuclear molecular gas in NGC 5793 with OH absorption

Y. Hagiwara[1], **P.J. Diamond**[2], **N. Nakai**[3], **and R. Kawabe**[3]

[1] Max-Planck-Insitut für Radioastronomie, Auf dem Hügel 69, 53121 Bonn, Germany (hagi@mpifr-bonn.mpg.de)
[2] MERLIN/VLBI National Facility, Jodrell Bank Observatory, Macclesfield Cheshire SK11 9DL, UK
[3] Nobeyama Radio Observatory, Nobeyama, Minamimaki, Minamisaku, Nagano, 384 − 1305, Japan

Received 3 December 1999 / Accepted 25 May 2000

Abstract. We have observed the nuclear region of an edge-on spiral galaxy NGC 5793 with VLBI in order to determine the morphology of the central continuum source at 6 and 18 cm and the distribution of OH molecular gas at 18 cm on parsec scales. NGC 5793, with a type 2 Seyfert nucleus, is known to have peculiar H_2O maser features in its center, indicating the presence of a rotating disk/torus (Hagiwara et al. 1997). Previous interferometric observations could not clarify both the continuum and OH gas structures due to low angular resolution (Gardner & Whiteoak 1986, Gardner et al. 1992). We find multiple continuum peaks forming a bent jet, though the observed peculiar morphology of the continuum source has no straightforward interpretation. We have also imaged the distribution of OH absorption toward the central continuum source. Due to the relative weakness of the continuum emission only the central continuum peak shows evidence of detectable opacity of the OH absorbing gas. The OH velocity field contour map reveals a velocity gradient of 8.7 km s^{-1} pc^{-1} nearly along the galaxy's optical axis. If we suppose that the observed OH velocity gradient is caused by simple solid rotation around the nucleus of the galaxy, the central binding mass is 4.2×10^8 M$_\odot$. The direction of the OH velocity field shows a reversal of a sense of rotation with respect to that of the outer galactic disk observed by CO $(1-0)$, implying the existence of an independent kinematical system in the central 10 parsec-scale region of the galaxy. Alternatively, the observed OH molecular absorption might possibly arise in the parsec-scale circumnuclear region of NGC 5793.

Key words: masers – ISM: kinematics and dynamics – galaxies: active – galaxies: ISM

1. Introduction

The discovery and subsequent sub-parsec scale studies of H_2O maser emission toward the nuclei of several galaxies have greatly improved our understanding of the circumnuclear regions of active galactic nuclei (AGN). Intense interferometric studies of the maser in the Seyfert/LINER galaxy NGC 4258, mainly using VLBI, provided a detailed description of a rotating circumnuclear disk in Keplerian motion with a radius of 0.13 pc, bound by a super massive black hole with a mass of 3.7×10^7 M$_\odot$ (Miyoshi et al. 1995; Greenhill et al. 1995; Nakai et al. 1993). Similar H_2O masing disks to those found in NGC 4258 have been identified in other AGN: NGC 1068 (Greenhill et al. 1996), NGC 3079 (Trotter et al. 1998; Sawada-Satoh et al. 2000) and NGC 4945 (Greenhill et al. 1997). These results imply that a sub-parsec or parsec-scale molecular disk/torus surrounding the nucleus is common in some narrow-line AGN and that their existence agrees well with the scheme which describes the unification of different types of AGN, originally proposed by Antonucci (1993).

VLBI observation of nuclear absorption lines is another method of studying the kinematics of the innermost region of circumnuclear gas. Gallimore et al. (1996a) found that the spectral profile and location of the HI absorption on 100 pc scales in NGC 1068 are consistent with those of H_2O masers which are seen around the nucleus and 30 pc further out along the jet. VLBI observations of NGC 1068 with sub-milliarcsecond angular resolution showed that nuclear H_2O masers are distributed with a radius of 0.65 pc and exhibit sub-Keplerian rotation (Greenhill et al. 1996). These observational facts strongly suggest that the structure and kinematics of the circumnuclear gas might be traced by absorption-lines as well as water masers.

NGC 5793 is an edge-on disk galaxy with a bright compact nucleus seen in radio continuum emission. Baan et al. (1998) classified the optical emission of NGC 5793 as being Seyfert type 2, which implies AGN activity. Assuming $H_0 = 75$ km s^{-1} Mpc^{-1}, the galaxy lies at a distance of 46 Mpc and 1 milliarcsecond (mas) corresponds to 0.23 pc. Gardner et al. (1992) made a European VLBI Network (EVN) image of the 21 cm continuum emission and found that the radio nucleus of NGC 5793 is unresolved with a radius of 16 mas, or about 4 pc on a linear scale. NRAO Very Large Array (VLA)[1] observations of the intense HI and OH absorption toward the nucleus demonstrated

Send offprint requests to: Y. Hagiwara

[1] The National Radio Observatory is a facility of the National Science Foundation operated under cooperative agreement with Associated Universities, Inc.

that the absorbing gas is located in a compact region around the nucleus (Gardner & Whiteoak 1986) and the wide velocity range of the HI and OH absorption profiles, $\sim 200\,\mathrm{km\,s^{-1}}$, is interpreted as being the result of a number of clouds of dense gas along the line of sight. Gardner et al. (1992) also performed HI absorption-line imaging with the EVN and concluded that three absorbing systems with different velocities are present, two of which are associated with the nucleus, while the third may be associated with gas flowing away from the nuclear region. However, insufficient spatial resolution made it difficult to determine whether or not the absorption really arises from the nucleus itself.

Single-dish observations detected intense H_2O maser emission from NGC 5793 (Hagiwara et al. 1997). The spectrum shows strong high-velocity features displaced by $\sim \pm 245\,\mathrm{km\,s^{-1}}$ on either side of the systemic velocity of the galaxy (V_{LSR} = 3442 km s^{-1}), accompanying weaker features are observed near the systemic velocity. Hagiwara et al. (1997) showed that the two velocity peaks of the H_2O systemic features seem to correspond to those of the OH absorption line peaks (Gardner & Whiteoak 1986), indicating a similar distribution of the H_2O and OH molecular gas in the galaxy. The parsec scale molecular absorption associated with AGN is a powerful tool for probing the inner layer of circumnuclear molecular gas which is considered as an energy source in the vicinity of a central engine. The nucleus of NGC 5793 also contains large opacity ($\tau > 2$) HI absorption covering a wide velocity range. According to the most recent HI absorption observation with VLBI, Pihlström et al. (2000) find that the atomic HI gas is not associated with the < 10 pc region close to the nucleus and suggest that it is probably associated with the outer galactic disk imaged using CO emission by Hagiwara (1998). In contrast, the OH molecular gas on parsec scales could trace a compact molecular gas disk/torus surrounding nucleus.

In this paper we describe the VLBI observations in Sect. 2, present the results of both continuum and OH absorption imaging in Sect. 3, and discuss the structure and kinematics of the nuclear region in Sect. 4.

2. Observation and analysis

Observations of NGC 5793 in both 18 cm continuum and OH spectral lines were made with the Very Long Baseline Array (VLBA) and the phased VLA on 1996 November 30. We observed the 1665 and 1667 MHz OH transitions of the $^2\prod_{3/2}$, J=3/2 ground-state in absorption toward the background radio continuum source. A continuous full track observation of 7.3 hours was performed, of which about 4 hours were spent on NGC 5793. The data were recorded in left circular polarization in four 8 MHz bands, corresponding to 1440 km s^{-1} in velocity, with 2 bit sampling. Each of the four 8 MHz IFs was subdivided into 512 spectral points, yielding a frequency resolution of 15.6 kHz, resulting in a velocity resolution of 2.82 km s^{-1}. In order to cover two OH absorption lines and the continuum we centered three IF bands on V_{LSR}= 3449, 3519, 3637 km s^{-1} and one on 3190 km s^{-1} (hereafter, all velocities are in the radio definition and with respect to LSR). These four Doppler velocity centers were referenced to the 1667 MHz main line. The first three IFs cover the absorption lines and were calibrated separately. However, only the first IF centered on 3449 km s^{-1} was used for absorption line imaging, the other two IFs were discarded. The fourth IF, an absorption-free band, was used for the continuum imaging.

Table 1. Adopted parameters of NGC 5793

R.A. (J2000)[a]	$14^h59^m24^s.76 \pm 0^s.01$
Dec. (J2000)[a]	$-16^\circ41'36''.14 \pm 0''.02$
Distance[b]	46 Mpc
Systemic Velocity (LSR)[c]	3442 ± 72 km s^{-1}
Type	Sb[d], Seyfert 2[e]
Position angle of the major axis[f]	150°
Inclination angle of the galactic disk[g]	73°

[a] Position of a radio core determined by VLA (Whiteoak & Gardner 1987). The coordinates are converted from those of B1950.
[b] Assuming H_0= 75 km s^{-1} Mpc $^{-1}$
[c] Hagiwara et al. (1997)
[d] de Vaucouleurs et al. (1976)
[e] Baan et al. (1998)
[f] Whiteoak & Gardner (1987)
[g] Roth (1994)

Subsequently, observations of 6 cm continuum emission with the VLBA alone were carried out on 1997 October 15. At 6 cm we observed in a phase-referencing mode, using the calibration source 1507−168 about 2 degrees away from NGC 5793, although we later found that NGC 5793 could be detected without phase-referencing. The total time of one cycle was 6 minutes; 4 minutes for NGC 5793 and 2 minutes for 1507−168, resulting in a total integration time on NGC 5793 of about 4 hours. The data were recorded in dual circular polarization in four 8 MHz bands with 2 bit sampling. Individual IFs with 16 spectral channels were obtained after correlation.

The system temperature and antenna sensitivity for each VLBA antenna at the relevant observing frequencies are 30−100 K and 11 Jy K^{-1}, respectively. The data were calibrated using the NRAO AIPS package. The delay and delay rate for each antenna were determined throughout the observation using 4C 39.25 and 1507−168. The absolute flux calibration of the VLA data was determined by observations of 3C 286. After the initial cleaned maps were obtained, self-calibration on the continuum sources at both wavelengths was employed, initially assuming point source models, to refine the phase solutions.

3. Results

3.1. Continuum

An 18 cm continuum image of NGC 5793 is shown in Fig. 1. The restoring beam size is 12.3×4.4 milliarcsecond (mas) in P.A. = -7.5°. The rms noise in the image is 0.21 mJy beam $^{-1}$.

Table 2. VLBI components in NGC 5793

Component	Peak flux density (mJy beam^{-1}) 18 cm	6 cm ($\theta_{\rm beam} = \theta_{\rm 18cm}$)[a]	Spectral Index $\alpha^{\rm 6\,cm}_{\rm 18\,cm}$ [b]
C1 (C)	308±19	91.1±4.6 (139±7.0)	–0.70±0.11
C1 (NE)	80.1±9.0	13.8±3.0 (25.0±1.3)	–1.0±0.16
C1 (SW)	12.8±6.4	< 0.22[c] (–)	–
C2(C)	18.0±0.9	5.1±0.3 (10.6±0.5)	–0.46±0.09
C2(W)	28.3±1.4	5.3±0.3 (12.2±0.6)	–0.72±0.10
C2(E)	(16.1)	11.1±0.6 (18.5±0.6)	(0.13)

[a] From an image convolved to the 18 cm beam size
[b] $\alpha; S_\nu \propto \nu^\alpha$
[c] 5σ upper limit value

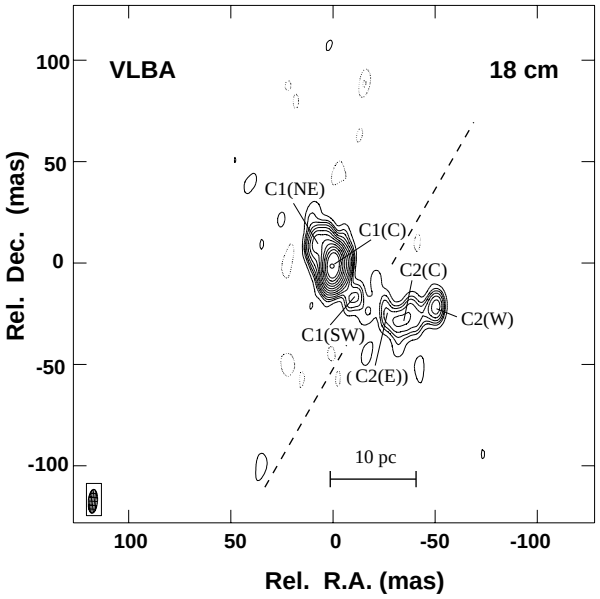

Fig. 1. A cleaned continuum image at 18 cm. The contour levels are -1.9, -1.0 (dashed), 1.0, 1.9, 2.7, 3.7, 5.2, 7.2, 10, 14, 19, 27, 37, 52, 72, and 100 % of the peak surface brightness of 308.4 mJy beam^{-1}. The synthesized beam of 12.3 × 4.4 milliarcsecond (mas) in P.A. = -7.5° is shown in the bottom left-hand corner. The position offsets are indicated within the frame. A dashed line shows the optical P.A. of the galaxy. The equivalent linear scale length in parsec is shown at the bottom.

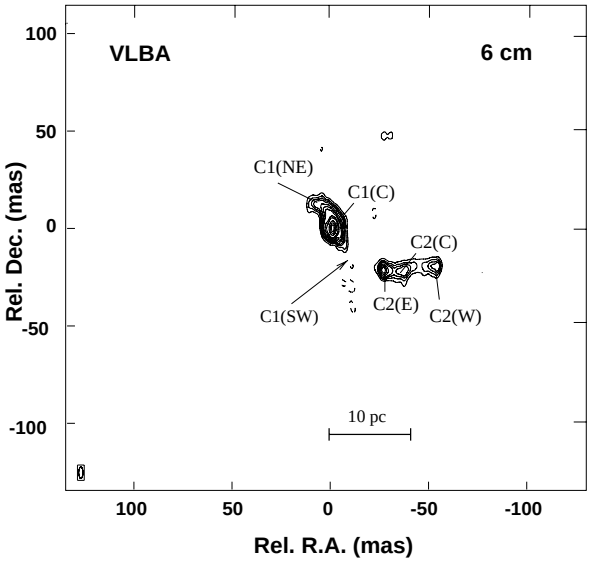

Fig. 2. A cleaned 6 cm continuum image. The contour levels are $-1\,(\rm dashed), 1, 2, 3, 4, 6, 8, 10, 15, 20, 40, 60, 80,$ and 100% of the peak surface brightness of 91.1 mJy beam^{-1}. The synthesized beam of 3.7 × 1.4 mas in P.A. = $-4.7°$ is shown in the left-hand corner.

The map shows a twisted radio structure split into two parts: a central bright component [C1(C)] with accompanying minor components [C1(NE) and C1(SW)] and a western elongated feature in P.A. $\simeq -70°$ (C2(C)), connected to a knot C2(W). The subcomponents C1(NE) and C1(SW) are almost symmetrically extended along a P.A. of 40° around the central peak of C1(C). The knots C1(NE), C2(C), and C2(W) may comprise a bending jet extending over nearly 18 pc. The peak flux density of 308 mJy beam^{-1} at C1(C) corresponds to a brightness temperature of 8.0×10^9 K. Brightness temperatures of other components range from 0.2 – 2.0 × 10^9 K.

Fig. 2 shows a 6 cm map with the restoring beam size of 3.7×1.4 mas in P.A. = $-4.7°$. The rms noise in the image is 0.043 mJy beam^{-1}. The peak flux density at C1(C) is 91 mJy beam^{-1} corresponding to a brightness temperature of 2.6×10^9 K, the brightness temperature of the other components is of the order of 10^8 K. The overall structure is similar to that at 18 cm but there are three important differences. First, component C1(SW) seen at 18 cm is not detected at 6 cm at all. Second, in the western elongation, we can clearly identify a new bright component C2(E) at its eastern edge, lying at a distance of 32 mas (7.4 pc) from the peak C1(C). Finally, the position of the peak of component C2(C) is offset northward by ~ 5 mas with respect to that at 18 cm.

The total flux density is 647 ± 9 mJy at 18 cm and 191 ± 3 mJy at 6 cm. Based on a comparison with the VLA B-configuration data (Gardner & Whiteoak 1986), we estimate that our images recover $\sim$ 65% of the total flux in the 18 cm map, but only $\sim$ 30% in the 6 cm map. Spectral indices of each component in Fig. 1 and 2 are measured between the two wavelengths and are summarized in Table 2. The 6 cm flux densities were obtained after convolving with the 18 cm beam.

3.2. The OH absorption

The phase and gain solutions obtained with one absorption-free IF channel were applied to the IF channel which contains both absorption and continuum emission. The continuum level was determined by averaging all channels. The continuum emission

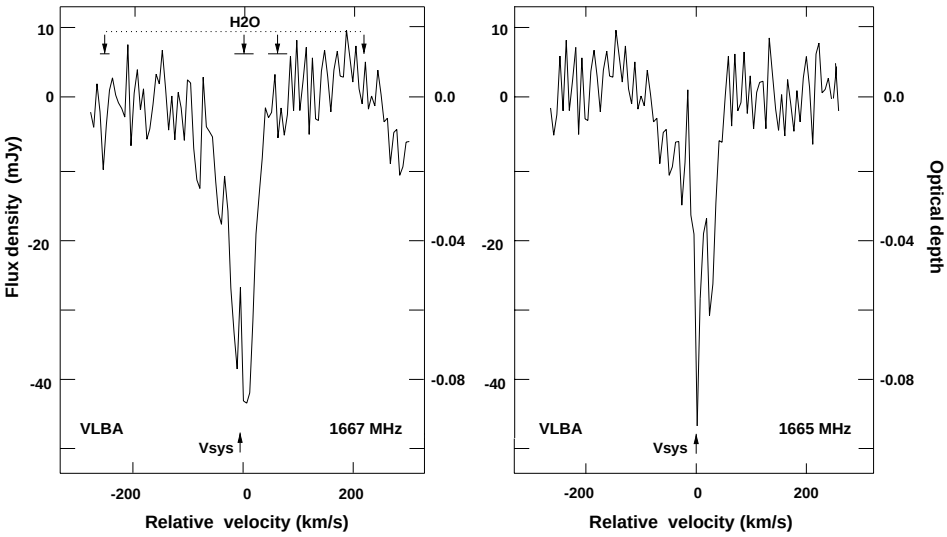

Fig. 3. The OH absorption spectra of 1667 (left) and 1665 MHz (right) with a spectral resolution of 31.3 kHz, or 5.6 km s^{-1}. The absorption intensities are labelled as flux density and optical depth. The relative LSR velocities are referred to the rest frequency of each OH transition at 1665.402 and 1667.359 MHz, or V_{LSR}= 3445 and 3454 km s^{-1}. The peak velocities (V_{LSR}= 3190, 3449, 3519, and 3677 km s^{-1}) and velocity ranges of the H_2O maser emission are indicated in the 1667 MHz frame by downward-pointing arrows and thick lines. The systemic velocity (V_{sys}) of 3442 km s^{-1} is denoted by an upward-pointing arrow.

Table 3. Parameters of the OH absorption feature

	VLA[a]	VLBA	
	1667 MHz	1665 MHz	1667 MHz
Optical depth (τ)			
Peak value	0.065±0.006	0.086±0.015	0.085±0.013
Gaussian fitted value[b]	–	0.066±0.016	0.080±0.012
Center Velocity (LSR)	3462 km s^{-1} [c]	3445±3 km s^{-1}	3454±4 km s^{-1}
Δ V (FWHM)	39.4 km s^{-1}	18±0.4 km s^{-1}	28.4±0.5 km s^{-1}
$\int \tau$dv	–	1.53 km s^{-1}	3.75 km s^{-1}

[a] Gardner & Whiteoak 1986; No published data for 1665 MHz
[b] Values derived from Gaussian fitted curves applied to original spectra in Fig. 3
[c] Converted to Radio LSR definition; V(radio heliocentric) – 8.0 km s^{-1}

was then subtracted from the spectral line visibility data cubes. Fig. 3 shows the 18 cm VLBA spectra with a spectral resolution smoothed to 5.6 km s^{-1}, toward the component C1(C); the two main OH transitions at 1665 and 1667 MHz are clearly seen in absorption. The 1667 MHz absorption spectrum was also previously detected with the VLA (Gardner & Whiteoak 1986). After continuum subtraction the spectra have been converted to optical depth using the above continuum level. In both transitions, several velocity features are detected, although some with poor signal-to-noise ratio. We fitted a single Gaussian component to the spectra shown in Fig. 3 in order to determine the optical depths, velocity centers, and velocity widths. The quality of the data did not warrant using additional components. The resultant values of opacity, integrated intensity and opacity intensities are listed in Table 3. The absorption velocity center (Gaussian fitted) at 1667 MHz is V_{LSR}= 3454 ± 4 km s^{-1} while the center velocity derived by Gardner & Whiteoak (1986) is V_{LSR}= 3462 km s^{-1}, which is very similar. The velocity centroid of the 1665 MHz absorption is 3796 ± 3 km s^{-1} (3454 km s^{-1}, referenced to the 1665 MHz transition), offset by 342 km s^{-1}. Note that the expected velocity difference of these two transitions is 351 km s^{-1}. The difference is probably due to sub-structure of the spectra. There is also weak evidence for 1665 and 1667 MHz OH absorption against components C1(NE) and C2(W), similar to that against C1(C), while the absorption against C1(SW) and C2(C) is too weak for us to estimate optical depths. However, the optical depths, line shapes, and velocity widths of the OH towards C2(W) do not show any significant difference from those towards C1(C). The absorption profiles show that the 1667 MHz feature is as deep as the 1665 MHz feature, though the thin component around at the systemic velocity in the 1665 MHz profile seems to contain a spurious noise. The hyperfine ratios of the peak OH optical depths and the OH opacity intensity derived by single Gaussian-fitting of the absorption line of each transition is 1.2 ± 0.1 and 2.5 ± 0.2 (see Table 3), showing significant deviation from the theoretical LTE ratio of 1.8 seen in galactic objects (Elitzur 1992).

Fig. 4 shows an OH absorption intensity image, integrated over the velocity span of 44.8 km s^{-1} at 1667 MHz. The integrated absorption flux density is −158 mJy km s^{-1} beam^{-1}. Significant OH absorption is detected mainly around the position of C1(C) as seen in Fig. 4. The absorption is apparently concentrated mostly around the position of C1(C) indicating that it traces the background continuum emission there. In Fig. 5, channel maps of the 1667 MHz OH absorption integrated every 5.6 km s^{-1} are shown; nine channel maps covering a velocity range −23 to 23 km s^{-1} with respect to the systemic velocity are displayed. The absorption shows a velocity gradient from north

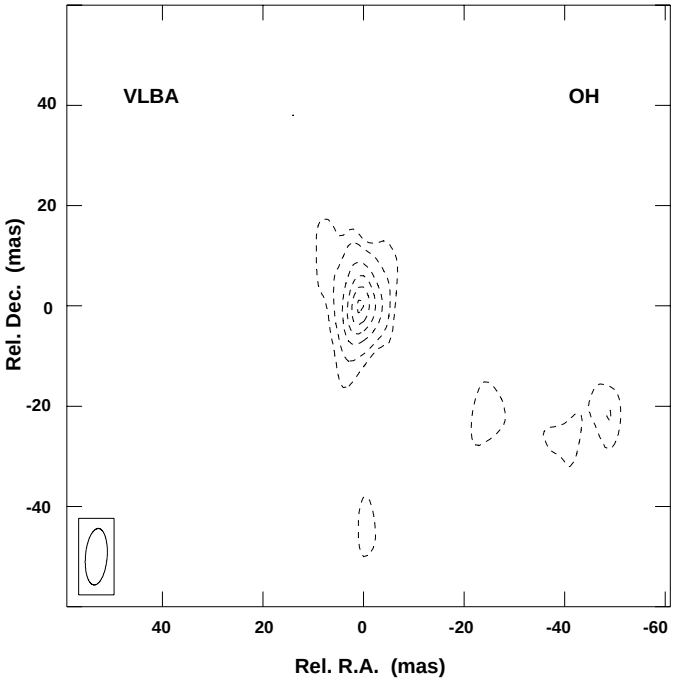

Fig. 4. An integrated intensity map of 1667 MHz OH absorption, integrated over the velocity width of 44.8 km s^{-1}. The integrated velocity range is V_{LSR}= 3422–3467 km s^{-1}. Dashed contour levels are 98, 80, 60, 40, 20, and 10% of the peak intensity of -158 mJy km s^{-1} beam^{-1}. The synthesized beam is shown in the left-hand corner. Significant absorption intensity is seen only around C1(C).

to south, starting approximately at V_{LSR}= 3430 km s^{-1} at 5 mas north of C1(C) and moving to V_{LSR}= 3459 km s^{-1} at 3 mas south of C1(C). In Fig. 6 a velocity contour map weighted with the OH absorption intensity (the first moment map) is shown. A velocity shift of about 40 km s^{-1} is seen over a distance of about 20 mas or 4.6 pc in the velocity range of $3425 < v < 3465$ km s^{-1} along P.A.$= 140°$, resulting in a velocity gradient of 8.7 km s^{-1} pc^{-1}. The range of this velocity gradient almost symmetrically spans the systemic velocity of NGC 5793, V_{LSR}= 3442 km s^{-1}. On the other hand, a velocity gradient in the 1665 MHz transition does not clearly have the trend as that seen in the 1667 MHz. This is mainly due to the low signal-to-noise ratio of the 1665 MHz line data; the spiky feature seen only in the 1665 MHz profile makes it difficult to deduce a reliable result.

4. Discussion

4.1. Nuclear continuum structure

We derive basic morphological and spectral properties of the parsec-scale radio structure of NGC 5793 from the 18 cm and 6 cm continuum maps and discuss the implications of these results. The continuum radio source has a core-jet structure that is typical for those seen in Seyfert galaxies and radio active galaxies. The VLBA data at both wavelengths suggest that the three components C1(C), C1(NE), and C2(W) have steep spectra of $-1.0 < \alpha < -0.7$ (using $S_\nu \propto \nu^\alpha$)(see Table 2). The component C2(E) in the 6 cm map could not be clearly identified in the 18 cm map. Estimating an 18 cm flux density of 16.1 mJy at the position of C2(E), its spectral index is 0.13 and is definitely inverted ($\alpha > 0$) or flat between these two wavelengths.

One might ask which component is the 'true' radio core of the galaxy. If we assume that the strongest continuum peak C1(C) is the core, the steep spectrum of C1(C) would likely be the result of a mixture of spectra from several components including a flat-spectrum radio core. Steep spectra in the range $-1.3 < \alpha < -0.5$ are generally observed in extragalactic extended radio sources (Barvainis & Lonsdale 1998), similar to those observed in the components in NGC 5793, suggesting that the continuum structure at C1(C) may still not be resolved on a scale of a few parsecs.

In contrast to the structure at 6 cm, the 18 cm image at the position of C2(E) does not show any counterpart corresponding to C2(E) at 6 cm. There are three possible explanations for this. We can account for the relative faintness of C2(E) at 18 cm by invoking a model of free-free absorption by an optically thick intervening gas disk/torus, which is highly inclined to the line of sight. In this case, the relative flatness of the C2(E) spectrum can be explained by there being a radio continuum core lying behind the obscuring gas along our line of sight. Therefore, the other possible candidate for the 'true' radio core is C2(E) in the 6 cm image. In that case, the central continuum structure containing C1(C), and the western extended emission containing C2(C) and C2(W), could be interpreted as jets that are directed from the highly inclined disk/torus, whose major axis lies at P.A. of $\sim 140°$, which is close to the galaxy's optical axis of $150°$. Alternatively, C2(E) could be an unobscured core and its lack of emission at 18 cm results from synchrotron self-absorption (e.g., Jones & Wehrle 1997). We will describe our investigations of these possibilities together with results of high-frequency observations with the VLBA, in a subsequent paper (Hagiwara et al. in preparation). Another possible explanation of the weakness of component C2(E) in the 18 cm map could be time variation of the flux density between the two observing epochs (almost one year) and, due to the relative faintness of 18 cm flux density, the spectrum of C2(E) apparently shows a flat or positive spectral index (see Table 2). If this was the case, the real spectrum at the C2(E) might be as steep as other components.

On balance, we suggest that C1(C), the most intense continuum peak, might be the position of the 'true' radio nucleus. C1(SE), C2(C), C2(W), and C2(E) could be a continuous jet ejected from the nucleus, while C1(NE) is the counter jet extending toward north-east. The bent structure of the jet close to C2(E) could be explained by deflection by gas clouds and the collimation axis of the jet being forced to change (e.g., NGC 1068: Gallimore et al. 1996b).

4.2. Properties of the OH absorption

Table 3 lists the single-Gaussian fitted parameters derived at C1(C) from the observed spectra in Fig. 3. The optical depth in the OH line at 1667 MHz, derived with the VLA in A-

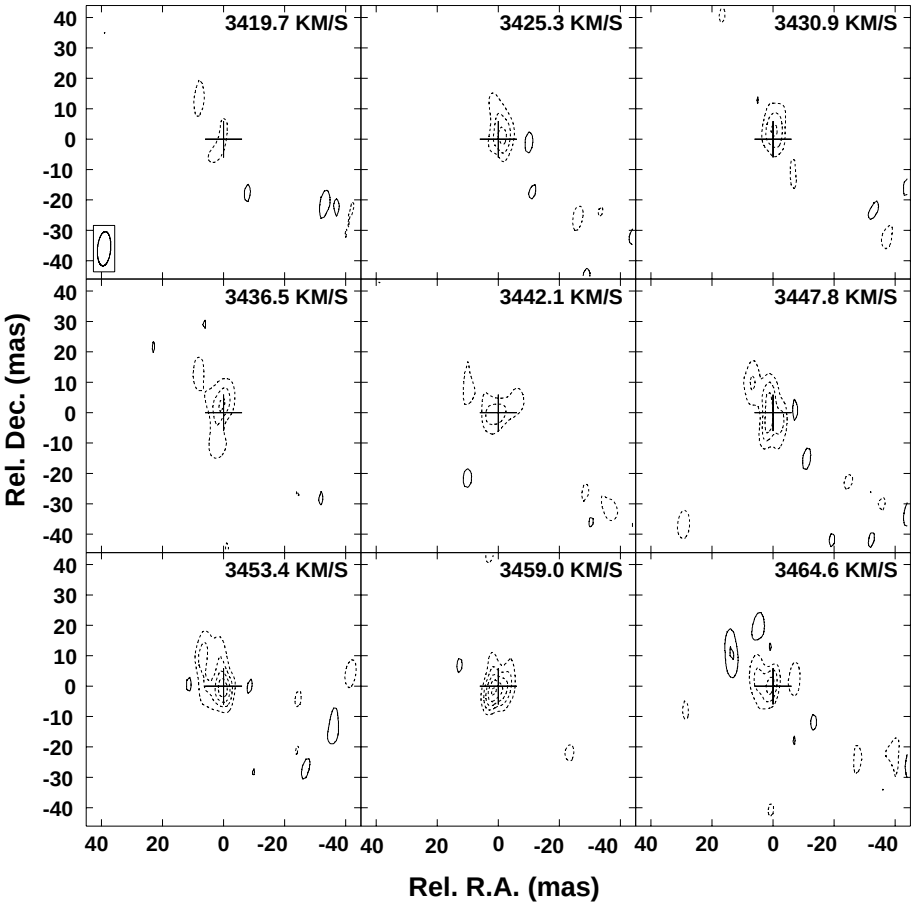

Fig. 5. Velocity channel maps of the 1667 MHz OH absorption, each integrated over 5.6 km s^{-1} intervals. The contour levels are at -25, -20, -15, -10, -5 (1σ) (dashed), 5, and 10 (solid) mJy beam^{-1}. Each map is labeled in the upper right hand corner with the velocity (V_{LSR}) at the center of each channel. The cross in each panel denotes the position of the phase center. The synthesized beam is shown in the upper-left corner panel.

configuration was 0.065 $\pm$ 0.006 (Gardner & Whiteoak 1986), while that derived from our VLBA data is 0.080 $\pm$ 0.012 at the Gaussian peak. The optical depth obtained by the smaller VLBA synthesized beam (HPBW = 0.012″) is consistent with that observed with the VLA (HPBW = 4″) within the errors. As mentioned in the previous section, we found little significant absorption at other positions in the continuum emission image, leaving the possibility that the foreground absorbing gas is spatially confined. The coincidence of these optical depth values within the errors does not contradict the above description. The velocity width of the absorption line in the 1667 MHz transition obtained with the VLBA (28.4 $\pm$ 0.5 km s^{-1}) is narrower by $\sim$ 30% than that observed with the VLA (39.4 km s^{-1}). This is attributed to the $\sim$ 35% missing flux density of the background continuum emission (which is resolved on parsec scales in our VLBA image). The extended radio continuum emission imaged by the VLA-A array, which is resolved in the 18 cm VLBA continuum image, seems to contribute several weaker OH velocity components which we cannot see in the VLBA profiles. It is interesting that compared with the HI absorption line widths from < 100 pc scale circumnuclear gas in Seyfert nuclei such as NGC 4151 (Mundell et al. 1995; Dickey 1986), the OH absorption of NGC 5793 is much narrower.

Assuming the gas to be optically thin (The optical depth value of 0.08 supports the fact that the OH absorbing gas is not optically thick.), the OH column density at 1667 MHz derived from the optical depth is $N(OH) = 2.2 \times 10^{14}\, T_{ex} \int \tau dv\, cm^{-2}$, where T_{ex} is the OH excitation temperature which typically ranges from 5–10 K (Elitzur 1992). Adopting the velocity integrated intensity of the absorption line in Table 3 the column density is 8.4×10^{15} cm^{-2} using T_{ex}= 10 K, which is in the range of the OH column densities found in molecular disks of nearby galaxies which have dusty nuclear regions (e.g., Baan & Haschick 1984, Baan et al. 1992).

4.3. Distribution and kinematics of the OH absorbing gas

The most intriguing result derived from our observations is that an OH velocity gradient symmetrically spanning the systemic velocity in the central region was detected. We determined a value of $\approx$ 8.7 km s^{-1} pc^{-1} for the velocity gradient across the continuum components of C1(C). Since the intensity distribution of the OH absorption (Fig. 4) (although it is difficult to make a map of OH optical depth because of the weakness of the continuum except at C1(C)) is well correlated with that of the background continuum emission (Fig. 1), the column density of OH does not vary across the continuum, suggesting that OH gas is distributed over a wider area than the continuum. Because the OH absorption is not seen in the outer region due to a lack of background continuum emission, it might be difficult to determine if the OH velocity field around C1(C) is caused by molecular gas associated with the nucleus. Nevertheless, in this

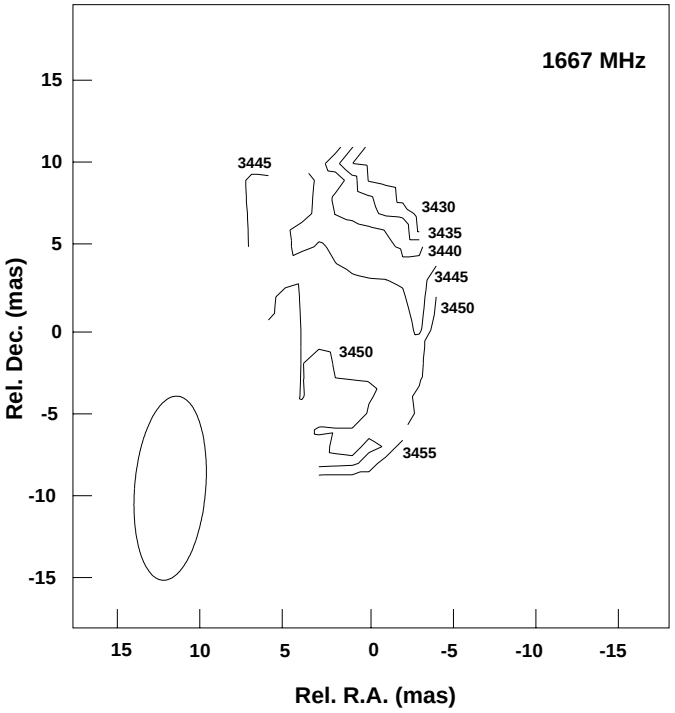

Fig. 6. The first moment map shows a distinct velocity field for the OH absorption at 1667 MHz covering the central region C1. Velocity contours are presented at 5 km s^{-1} intervals, and velocities are labeled in units of km s^{-1} ($V_{\rm LSR}$). The 18 cm synthesized beam is plotted in the bottom left corner. The velocity gradient is clearly seen nearly along the major axis of the galaxy ranging $V_{\rm LSR}$= 3430–3455 km s^{-1}.

section we examine the kinematical properties of the OH gas, making use of the results of H_2O maser and CO molecular gas observations.

High-resolution millimeter observations of CO (J = 1−0) with the Nobeyama Millimeter Array (NMA) found a rotating molecular gas structure in the central region of the galaxy with a radius of $\sim$ 1 kpc along P.A. = $\sim$ 140° spanning $V_{\rm LSR}$= 3305–3661 km s^{-1} (Hagiwara et al. 1997, Hagiwara 1998). In this paper, the OH velocity gradient shows a reversal of the sense of rotation observed in the central region of $\sim$ 10 pc. This suggests that the OH absorbing gas that we detected with the VLBA is kinematically distinct from the outer disk observed in CO. This kind of compact gaseous subsystem which is kinematically independent from the larger scale galactic molecular gas disk has been observed in other galaxies, such as, NGC 4826 (Braun et al. 1992), NGC 253 (Anantharamaiah & Goss 1996), and NGC 3079 (Sawada-Satoh et al. 2000).

In the following we consider that the velocity gradient observed around C1(C) might arise from a rotating molecular disk with a radius (r) centered on the nucleus. In order to explain the H_2O spectrum showing systemic and red- and blue-shifted features in NGC 5793, Hagiwara et al. (1997) proposed a nearly edge-on circumnuclear molecular disk/torus with a radius of $r > 4 - 20$ pc and a rotation velocity of $V_{\rm rot}$ = 245 km s^{-1}. If we suppose that absorbing OH gas is located in the same molecular disk/torus, the observed velocity gradient (dV/dl) along the major axis of P.A. = 140° can be expressed as follows;

$$\frac{dV}{dl} \simeq \frac{d(V_{rot}\ \theta\ sini)}{d(r\theta)} = \frac{V_{rot}}{r}, \quad (1)$$

where l is the projected distance from the source center, i = 73° is an inclination of the molecular rotating disk, and sin$\theta \approx \theta$ is adopted (Nakai 1995). We adopt the inclination of the OH disk is to be 73°, that of galaxy's optical disk. For $V_{\rm rot}$ = 245 km s^{-1} and dV/dl = 8.7 km s^{-1} pc^{-1}, r is estimated to be about 28 pc. Using this value for the radius of a molecular disk/torus around C1(C), the mass confined within the disk is $4.2 \times 10^8\ M_\odot$. This estimate is larger by approximately a factor of three than the mass previously derived from water maser profiles (Hagiwara et al. 1997), because they adopted r = 10 pc. We must note, however, that the mass estimate will depend on the assumed inclination angle of the rotating gas disk. The fact that H_2O maser features were preferentially observed in the edge-on molecular disks supports our assumption (e.g., Miyoshi et al. 1995). On the other hand, the gas mass of molecular hydrogen in the outer disk, that is determined from the CO intensity estimated from the CO profile, is $8.0 \times 10^9 M_\odot$ (Hagiwara 1998). The OH gas mass within a radius of 10 mas or 2.3 pc from the continuum peak corresponds to about 5% of that in the CO disk with a radius of $\sim$ 1 kpc, implying that the density of observed OH gas is significantly greater than that of the outer molecular gas disk.

One of our motivations for this observation was to investigate whether or not the OH absorption in NGC 5793 takes place in the same molecular cloud that contains the H_2O maser. The centroid velocities of the H_2O emission peaks at $V_{\rm LSR}$= 3449 and 3519 $\pm$ 5 km s^{-1} are close to those of the OH absorption lines observed with the VLA (Gardner & Whiteoak 1986), although only the OH feature at 3449 km s^{-1} was detected in our VLBA observation (the 1667 MHz spectrum of Fig. 3). The 3519 km s^{-1} absorption feature, which is weaker than that at 3449 km s^{-1}, was not clearly detected, probably because the extended background continuum necessary to observe it in absorption is resolved with the VLBA. Another OH velocity component was found in the velocity range of the H_2O maser feature at 3449 km s^{-1}, however there is no clear evidence for a rotating OH molecular disk/torus around the nucleus or a relationship with the proposed water maser disk proposed in Hagiwara et al. (1997). The large value of the OH column density along the line of sight, the high mass density of the observed absorbing cloud and the existence of the velocity gradient around the nuclear region, dynamically independent from the outer galactic disk, demonstrate that the observed OH absorption probably arises from the dense molecular gas in the circumnuclear region of NGC 5793.

5. Summary

We have mapped the distribution of continuum emission and of the OH absorption at 1667 MHz in the Seyfert galaxy NGC 5793 on parsec scales with VLBI. The observed structure of the OH

absorption shows a velocity gradient across the continuum structure of C1(C), the velocity range symmetrically spanning the systemic velocity. The direction of the OH velocity gradient is inconsistent with that of rotation of the kiloparsec scale CO disk of the galaxy, though the P.A. of these two axes are nearly aligned: we have discovered a counter-rotating gaseous component in the inner region on scale of 10 parsecs. If circular rotation across C1(C) is invoked to explain the velocity gradient, based on the assumption that the H_2O maser emission is from the same gas, the binding mass is $4.2 \times 10^8 M_\odot$. This value corresponds to nearly 5% of the molecular gas mass existing in the kiloparsec-scale galactic disk. The interpretation of the observed OH absorption distribution is not unique. The OH absorption could arise from dense molecular gas in the 10 parsec scale circumnuclear disk/torus or from spatially extended diffuse molecular gas on kiloparsec scales in the galactic disk, although we favour the former explanation. The structure and spectra of the continuum components are difficult to interpret. However, C1(C) is the strongest component and is that against which the strongest OH absorption occurs, suggesting that C1(C) is the core. More data are required to resolve this issue.

Acknowledgements. The authors acknowledge helpful discussions with and comments from Drs. S. Kameno, M. Miyoshi, S. Deguchi, J. Conway, K. Menten and W. Baan. Y.H. thanks the Foundation for the Promotion of Astronomy of Japan for travel support to visit NRAO, Socorro for the data analysis. We would also like to thank the referee, Huib Jan van Langevelde for a careful and critical reading of the text. The National Radio Astronomy Observatory is operated by Associated Universities, Inc. (AUI), under cooperative agreement with the National Science Foundation. This paper represents a part of Y.H. 's Ph. D thesis, submitted to the Graduate University for Advanced Studies, Mitaka, Japan.

References

Anantharamaiah K.R., Goss W.M., 1996, ApJ 466, L13
Antonucci R., 1993, ARA&A 31, 473
Baan W. A., Haschick A. D., 1984, ApJ 279, 541
Baan W. A., Rhoads J., Haschick A. D., 1992, ApJ 401, 508
Baan W. A., Salzer J. J., LeWinter, R. D., 1998, ApJ 509, 633
Barvainis R., Lonsdale C., 1998, AJ 115, 885
Braun R., Walterbos R. A. M., Kennicutt R. C., Jr., 1992, Nat 360, 442
de Vaucouleurs G., de Vaucouleurs A., Corwin H. G.Jr., 1976, Second Reference Catalogue of Bright Galaxies, University of Texas, Austin, TX, US
Dickey J.M., 1986, ApJ 300, 190
Elitzur M., 1992, Astronomical Masers (Kluwer Academic Publishers)
Gallimore J. F., Baum S. A., O'Dea C.P., et al., 1996a, ApJ 462, 740
Gallimore J. F., Baum S. A., O'Dea C. P., 1996b, ApJ 464, 198
Gardner F. F., Whiteoak J. B., 1986, MNRAS 221, 537
Gardner F. F., Whiteoak J. B., Norris R. P., et al., 1992, MNRAS 258, 296
Greenhill L. J., Jiang D. R., Moran J. M., et al., 1995, ApJ 440, 619
Greenhill L. J., Gwinn C. R., Antonucci R., et al., 1996, ApJ 472, L21
Greenhill L. J., Moran J. M., Herrnstein J. R., 1997, ApJ 481, L23
Hagiwara Y., Kohno K., Kawabe R., et al., 1997, PASJ 49, 171
Hagiwara Y., 1998, High-Resolution Interferometric Study of Circumnuclear Gas in Radio-Active Galaxies, Ph. D thesis, The Graduate University for Advanced Studies, Mitaka, Japan.
Jones D. L., Wehrle A. E., 1997, ApJ 484, 186
Miyoshi M., Moran J. M., Herrnstein J. R., et al., 1995, Nat 373, 127
Mundell C. G., Pedlar A., Baum S. A., et al., 1995, MNRAS 272, 355
Nakai N., Inoue M., Miyoshi M., 1993, Nat 361, 45
Nakai N., 1995, In: Sato K, Suginohara T, Sugiyama N (eds.), The Cosmological Constant and the Evolution of the Universe, Universal Academy Press, Inc., Tokyo, Japan, p. 113
Pihlström Y. M., Conway J. E., Booth R. S., et al., 2000, A&A 357, 7.
Roth J., 1994, AJ 108, 862
Sawada-Satoh S, Inoue M., Shibata K. M., et al., 2000, PASJ 52, 421
Trotter A. S., Greenhill L. J., Moran J. M., et al., 1998, ApJ 495 740
Whiteoak J. B., Gardner F. F., 1987, Proc. Astro. Soc. Aust. 7, 88